A Journal of the Gesellschaft Deutscher Chemiker
Angewandte Chemie
GDCh
International Edition
www.angewandte.org

Accepted Article

Title: Engineering Sensitized Photon Upconversion Efficiency via Nanocrystal Wavefunction and Molecular Geometry

Authors: Shan He and Kaifeng Wu

To be cited as: *Angew. Chem. Int. Ed.* 10.1002/anie.202009066

Link to VoR: https://doi.org/10.1002/anie.202009066

WILEY-VCH

Engineering Sensitized Photon Upconversion Efficiency via Nanocrystal Wavefunction and Molecular Geometry

*Shan He, Runchen Lai, Qike Jiang, Yaoyao Han, Xiao Luo, Yuyang Tian, Xue Liu and Kaifeng Wu**

[*] Dr. S. He, Dr. R. Lai, Y. Han, Dr. X. Luo, Y. Tian, X. Liu, Prof. Dr. K. Wu
State Key Laboratory of Molecular Reaction Dynamics, Dynamics Research Center for Energy and Environmental Materials, Dalian Institute of Chemical Physics, Chinese Academy of Sciences, Dalian, Liaoning 116023, China
E-mail: kwu@dicp.ac.cn
Q. Jiang
State Key Laboratory of Catalysis, Dalian Institute of Chemical Physics, Chinese Academy of Sciences, Dalian, Liaoning 116023, China
Y. Han
University of the Chinese Academy of Sciences, Beijing 100049, China

Supporting information for this article is given via a link at the end of the document.

Abstract: Triplet energy transfer from inorganic nanocrystals to molecular acceptors has attracted strong attention as a promising approach to high-efficiency photon upconversion that is important for energy-related applications. Because energy transfer is a donor-acceptor interfacial process, it is essential to simultaneously engineer the nanocrystal and molecular parameters in order to uncover unified physical principles that are transferable among different systems. Here we study this problem using $CsPbBr_3$ and CdSe nanocrystals as triplet donors and carboxylated anthracene isomers as acceptors. We find that the position of the carboxyl anchoring group on the molecule dictates the donor-acceptor coupling to be either “through-bond” or “through-space”, while the relative strengths of the two coupling pathways is controlled by the “wavefunction-leakage” of nanocrystals that can be quantitatively tuned by nanocrystal sizes or shell thicknesses. By simultaneously engineering molecular geometry and nanocrystal wavefunction, energy transfer and photon upconversion efficiencies of a nanocrystal/molecule system can be improved by orders of magnitude.

Introduction

Sensitization of molecular spin-triplet states is essential for many applications, including but not limited to organic photoredox catalysis, photodynamic therapy, room temperature phosphorescence, and triplet-triplet annihilation based photon upconversion.[1] Development of efficient triplet sensitizers has thus been an important subject of research in photochemistry.[1-2] It was until very recently that colloidal semiconductor nanocrystals (NCs), which have been under study for over three decades,[3] were recognized as excellent triplet sensitizers.[4] Compared to traditional organic or organometallic sensitizers, NCs have many advantages such as negligible intersystem crossing energy loss, strong light absorption and facile spectral tunability.[4f-h, 5]

In the past few years, researchers have systematically investigated how the NC parameters, such as sizes[4i, 6] and shell thicknesses[7], influence the efficiency of triplet energy transfer (TET) from NCs to molecular acceptors. For example, the NC size effect in triplet sensitization has been reported for CdSe NCs,[6a] PbS(Se) NCs[6b] and more recently $CsPbBr_3$ perovskite NCs.[4i, 6c] In general, a decrease in the NC size can enhance both the driving force[6b] and the electronic coupling[4i, 6c] required for TET, which increases the efficiencies of TET and photon upconversion based on it. Besides NC parameters, molecular design also has an important impact on TET. The efficiencies of TET from CdSe NCs to anthracene acceptors functionalized with carboxylate, dithiocarbamate or diphosphate groups were found to be very different.[8] Interestingly, the substitution position of the functional group on the molecule is important as well. For example, the photon upconversion efficiencies of CdSe NCs with different carboxylated anthracene isomers differed by more than 10-fold.[8a] These effects were often tentatively attributed to electronic coupling strengths (orbital overlaps) between NCs and molecular acceptors.[8a] However, the exact mechanism by which the electronic coupling differs remains unclear.

Considering that TET occurs across the donor-acceptor interface, it is essential to simultaneously engineer the nanocrystal and molecular parameters in order to uncover physical principles that are transferable among various systems. Such unified principles, however, are still lacking in the field, which is the motivation of the current work. Here we study TET from $CsPbBr_3$ NCs of varying sizes to carboxylated anthracene isomers, using a combination of static and time-resolved spectroscopy, and investigate their impact on photon upconversion efficiencies. $CsPbBr_3$ perovskite NCs were chosen because of their unique “defect-tolerance” and distinctive spectroscopic features well suited to TET studies.[4i, 4j, 6c, 9] We find that the NC-molecule coupling mechanisms are “through-bond” and “through-space” when the carboxyl and anthracene moieties in the molecule are co-planar or orthogonal, respectively. The relative strength of the two coupling mechanisms is controlled by the “wavefunction-leakage” of NCs, with small-size, strongly-confined NCs favoring the “through-space“ mechanism. Such a wavefunction-engineering strategy is further validated using CdSe@ZnS core@shell NCs of varying shell thicknesses.

Results and discussion

We first examined the performances of triplet-triplet annihilation photon upconversion (TTA-UC) using $CsPbBr_3$ NCs with surface-anchored anthracene carboxylic acid (ACA) ligands. Fig. 1a shows the UV-vis absorption spectra of three different-sized $CsPbBr_3$ NCs prepared using a hot injection method;[4i, 10] see Methods in the Supporting Information (SI) for details. The lowest energy absorption peaks of these samples are situated at 450, 454 and 468 nm, which are used label the NCs in the following. According to their transmission electron microscope (TEM) images (Fig. S1), these samples correspond to NC sizes

10.1002/anie.202009066

(edge lengths) of ~3.2, 3.4 and 4.3 nm, respectively, which are consistent with the previously-reported sizing curve for $CsPbBr_3$ NCs.[11] The size distributions of these NCs are in the range of 4.6 to 9.4% (Fig. S1), resulting in well-resolved, multiple excitonic absorption peaks in Fig. 1a.

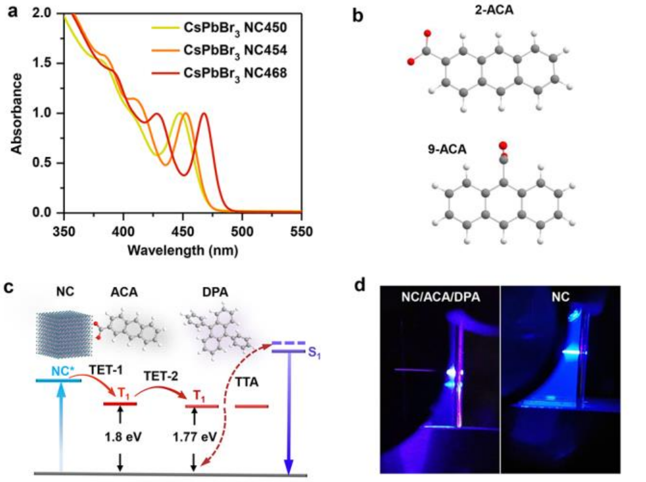

Figure 1. $CsPbBr_3$ perovskite NC-ACA systems for photon upconversion. (a) UV-vis absorption spectra of $CsPbBr_3$ NCs with lowest exciton peaks at 450 (yellow), 454 (orange) and 468 nm (red). The peak positions are used to label the samples. (b) Chemical structures of the 2-anthracene carboxylic acid (ACA) and 9-ACA isomers. Gray: C; white: H; red: O. (c) Schematic and electronic level diagram of the system for photon upconversion (UC). The system comprises ACA-anchored $CsPbBr_3$ NCs and diphenylanthracene (DPA) dispersed in deaerated hexane solvent. (d) Pictures of a typical NC/ACA/DPA mixture (left) and a free NC solution (right) under 443 nm excitation. The UC light can be seen through a short-pass filter (left).

The chemical structures of the two ACA isomers, 2-ACA and 9-ACA, are shown in Fig. 1b. They were anchored onto NC surfaces using a ligand exchange procedure (Methods).[4b, 12] The numbers of 2-ACA and 9-ACA ligands per NC were controlled to be similar for each sample; these numbers are ~198, 175 and 255 for NC450, NC454 and NC468, respectively (Table S1). In this way, any difference between the TET or TTA-UC efficiencies of each NC anchored with 2-ACA and 9-ACA ligands is not caused the difference in the number of ACA molecules. Note that, because the carboxyl group is known to be deprotonated upon anchoring the molecules onto NC surfaces,[13] we show the deprotonated forms of the ACA molecules and all the following discussions on ACA refer to deprotonated ACA. Density functional theory (DFT) optimizations of the ground-state geometries indicate that the dihedral angles between the carboxylate and anthracene moieties are close to 0 and 90 degrees, respectively, for 2-ACA and 9-ACA (Fig. 1b). This is consistent with previous reports and can be rationalized by that a large steric hindrance effect between the carboxylate group and the peripheral H atoms on anthracene exists in 9-ACA but not in 2-ACA.[14] As a result, there is a resonance effect (*i.e.*, wavefunction delocalization) between the carboxylate and anthracene moieties for 2-ACA but not for 9-ACA, which explains the red-shift (lower energy) of the absorption onset of 2-ACA compared to that of 9-ACA (Fig. S2). We will illustrate later that the resonance effect plays a key role in the electronic coupling mechanism between NCs and ACA.

For TTA-UC measurements, we combined ACA-anchored $CsPbBr_3$ NCs and diphenylanthracene (DPA) in hexane solution, with the later acting as effective annihilators.[4d, 4k, 6a, 15] As schematically shown in Fig. 1c, photoexcited NCs sensitize ACA triplet (^{3}ACA*; E_T ~ 1.83 eV) through a TET process (TET-1); the ACA ligands further pass the triplet energy to DPA molecules (E_T ~ 1.77 eV) in the solution (TET-2) which emit upconverted photons via TTA. Because of a weak exchange interaction on the order of meV in $CsPbBr_3$ NCs,[16] we can assume that the lowest exciton energy determined from the absorption spectrum is the triplet energy, which is 2.76, 2.73 and 2.65 eV for NC450, NC454 and NC468, respectively. Thus, the driving forces for TET from NCs to ACA ligands are very strong.

In order to efficiently excite the $CsPbBr_3$ NCs but not ACA (absorption spectra in Fig. S2) and DPA (absorption spectrum in Fig. S3) in the mixture, we used a continuous wave (*cw*) laser of 443 nm; see SI for details. As shown in Fig. 1d, for the NC/ACA/DPA mixture, the UC light can be seen through a short-pass filter that cuts off the laser light and the residual NC emission. Fig. S4 shows the PL spectra of NC/ACA/DPA systems with different NC sizes under 443 nm excitation, where both the residual emission of NCs and the UC emissions can be observed. The UC emission intensity increases with excitation power first quadratically and then linearly (Fig. S5), which is a typical feature of sensitized TTA-UC.[1]

Table 1. TTA-UC and TET efficiencies of $CsPbBr_3$ NC/ACA systems.

	NC450		NC454		NC468	
	2-ACA	9-ACA	2-ACA	9-ACA	2-ACA	9-ACA
Φ'_{UC} (%)	13.0	5.3	12.4	3.4	6.9	0.6
Q_{PL} (%)	98.1	35.0	96.0	21.7	84.8	6.7
$Q_{TR\text{-}PL}$ (%)	97.4	35.7	95.7	22.2	85.6	6.9

The calculated UC quantum yields (Φ'_{UC}) are summarized in Table 1; calculation details are provided in the SI. We can identify three important trends when comparing these yields. First, the UC yields generally decrease with increasing NC sizes. Considering that the exciton energies of all three NCs (2.65-2.76 eV) are much higher than the triplet energy of ACA (1.83 eV), the size-dependent electronic coupling for TET from NCs to ACA is believed to be responsible for the observed trend.[4i] Secondly, for each NC sample, NC/2-ACA has a higher UC yield than NC/9-ACA, which is exactly opposite to previous observation for CdSe NCs.[8a] Last but not the least, the UC yields of NC/9-ACA samples display a stronger size-dependence than those of NC/2-ACA. As a result, the yield difference increases from ~2.4-fold for NC450 to 11.5-fold for NC468. Note that we also measured TTA-UC using 1-ACA ligand, another common ACA isomer, and the UC yields always fall in between the results of 2-ACA and 9-ACA (Table S2). In order to understand these trends, we performed detailed static and time-resolved spectroscopic experiments.

The static PL spectra in Fig. S4 already imply the key process determining the TTA-UC yields. The UC emission is strong when the NC emission is efficiently quenched. The NC emission quenching efficiencies by ACA (Q_{PL}) are tabulated in Table 1, which reveals a clear correlation between Q_{PL} and Φ'_{UC}. Thus, Φ'_{UC} is mainly determined by the efficiency of TET from $CsPbBr_3$ NCs to ACA ligands (TET-1 in Fig. 1c), and the change in NC sizes or ACA isomers mainly affects this TET efficiency. Time-resolved PL measurements were also used to calculate the quenching rates and efficiencies (see Fig. S4 and SI for

10.1002/anie.202009066

details). The quenching efficiencies calculated in this way ($Q_{TR\text{-}PL}$) agree well with the static PL quenching efficiencies (Table 1). The quenching rates, *i.e.*, TET rates (k_{TET}), are in the range of 0.05 to 6.45 ns^{-1}. We note that, because 9-ACA quenches the PL of NC468 by only 6.7%, the PL quenching caused by trap states introduced in the ligand exchange process is believed to be negligible, consistent with previous studies.[4b, 9a]

Because time-resolved PL only measures the excited state decay of NCs, we also performed transient absorption (TA; see Methods in the SI) experiments to directly observe both the excited state decay of NCs and formation of ACA triplets.[4b] Figs. 2a and 2b show the TA spectra of NC454 in the absence and presence of 2-ACA ligands, respectively, measured under the same conditions (460 nm pump). The TA features of free NCs decay away within ~10 ns due to radiative and/or nonradiative recombinations of band edge electrons and holes. In the presence of 2-ACA, the TA features of NCs show rapid decay within ~1 ns, and meanwhile, a new absorptive feature at ~430 nm emerges which can be assigned to the $T_1 \rightarrow T_n$ transition of ACA triplets (^{3}ACA*).[4b] This triplet spectrum becomes especially obvious on the μs timescale when the NC features completely disappear (Fig. 2b). In line with TR-PL measurements, 9-ACA quenches the NC TA features much more slowly than 2-ACA, as clearly shown by the comparison of the XB kinetics probed for NC454, NC454/2-ACA and NC454/9-ACA in Fig. 2c.

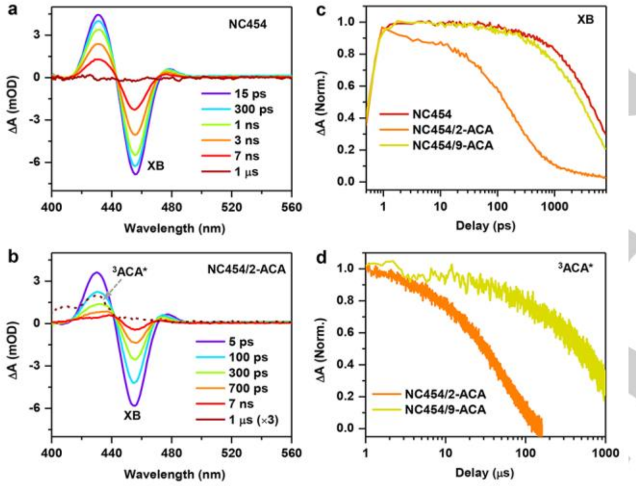

Figure 3. Transient absorption measurements. TA spectra of (a) $CsPbBr_3$ NC454 and (b) NC454/2-ACA at indicated time delays following the excitation by 460 nm pulses. The triplet absorption feature (^{3}ACA*) of 2-ACA is amplified by a factor of 3 for clarity. (c) TA kinetics probed at the XB features of free NCs (red), NC/2-ACA (orange) and NC/9-ACA (yellow). (d) Triplet decay kinetics of 2-ACA (orange) and 9-ACA (yellow) sensitized by NC454.

Interestingly, the lifetimes of sensitized 2-ACA and 9-ACA triplets are remarkably different. As shown in Fig. 2d, the 1/e decay times are ~50 μs and 1 ms for 2-ACA and 9-ACA, respectively, with the latter value consistent with the literature result.[4b] The reason for the difference is not clear yet, but is likely associated with the resonance effect between the carboxylate and anthracene moieties existing in 2-ACA but not in 9-ACA. The resonance effect renders the excited state of 2-ACA susceptible to more nuclear degrees of freedom. The 20-fold longer triplet lifetime of 9-ACA than 2-ACA, combined with the higher TTA-UC efficiencies of NC/2-ACA systems, further supports that the efficiency of TET from NCs to ACA ligands (TET-1) rather than from ACA ligands to DPA (TET-2) determines the TTA-UC efficiency. Otherwise, a longer triplet lifetime of 9-ACA should result in a higher TET-2 efficiency and thus a higher TTA-UC efficiency. TA spectra of NC450 and NC468 and their NC/ACA complexes are shown in Figs. S6 and S7 and the overall observations are similar to those of NC454.

The large difference between the rates of TET from $CsPbBr_3$ NCs to 2-ACA and 9-ACA cannot be attributed to energetics (driving forces), as the excited state energies and redox potentials of the two ACA isomers are very similar (Fig. S8). This is consistent with the conclusion from a previous study of TET from CdSe NCs to ACA isomers.[8a] Interestingly, however, as we mentioned above, for CdSe NCs TET to 9-ACA is more efficient than to 2-ACA.[8a] Rationalizing the opposite trends observed for $CsPbBr_3$ and CdSe NCs might be a key to understanding TET from NCs to surface-anchored acceptors.

We approach this problem by analyzing the fundamental photophysics of semiconductor NCs. The CdSe NCs used in previous studies often have the lowest energy absorption peak at ~500-520 nm, corresponding to a NC diameter of ~2.3-2.5 nm.[4b, 8a] The sizes of $CsPbBr_3$ NCs used here are in the range of 3.2-4.3 nm. Because the Bohr exciton diameters of bulk CdSe and $CsPbBr_3$ are ~11.2 (ref[17]) and 7 nm (ref[18]), respectively, CdSe NCs are more strongly quantum-confined than $CsPbBr_3$ NCs. Quantum confinement strongly affects the electronic coupling between NCs and surface-anchored acceptors because more strongly confined NCs tend to have higher carrier wavefunction amplitudes on NC surfaces.[3a, 19] The difference in surface wavefunction amplitudes and associated electronic coupling strengths with surface-anchored acceptors might be responsible for the opposite trends observed for CdSe and $CsPbBr_3$ NCs.

In order to verify the wavefunction argument, we systematically tune wavefunction amplitudes on CdSe NC surfaces by coating them with ZnS shells of varying thicknesses[20]. Because of a type-I band alignment between CdSe and ZnS, the ZnS shell functions as a tunneling layer for charge/triplet energy transfer from the CdSe core to ACA ligands. Details for the synthesis of CdSe@ZnS core@shell NCs are provided in Methods in the SI. The shell thicknesses were controlled to correspond to 0.5, 1 and 2 monolayers (MLs) of ZnS; see TEM images in Fig. S9. UV-vis absorption spectra of the core and core@shell NCs are shown in Fig. S10. The lowest energy absorption peak only slightly shifts from 505 to 515 nm (48 meV shift) upon coating the core with 2 MLs of ZnS. Thus, these core@shell NCs can be used to control wavefunction amplitudes on NC surfaces with the energetics remaining virtually unchanged.

Table 2. TET efficiencies of CdSe@ZnS NC/ACA systems.

	CdSe		**CdSe@0.5ZnS**	
	2-ACA	**9-ACA**	**2-ACA**	**9-ACA**
Q_{PL} (%)	72.9	89.2	33.6	41.2
$Q_{TR\text{-}PL}$ (%)	70.9	87	34.1	41
	CdSe@1ZnS		**CdSe@2ZnS**	
	2-ACA	**9-ACA**	**2-ACA**	**9-ACA**
Q_{PL} (%)	20.6	13	15.8	3.8
$Q_{TR\text{-}PL}$ (%)	19.4	12.1	15.4	4.3

ACA ligands were functionalized onto CdSe@ZnS core@shell NC surfaces in a similar way as $CsPbBr_3$ NCs. The average numbers of 2-ACA and 9-ACA ligands per NC are calculated to be ~13, 11, 10 and 13 for CdSe, CdSe@0.5ZnS, CdSe@1ZnS and CdSe@2ZnS NCs, respectively (Table S1). These numbers are in general one order of magnitude lower than those for $CsPbBr_3$ NCs, likely because the surface of $CsPbBr_3$ NCs is highly dynamic,[21] allowing more ACA molecules to bind to their surface through ligand exchange.

Because TET from CdSe NCs to ACA ligands has already been well established in the literature using TA,[4b, 8a] here we use PL (Fig. S11) and TR-PL (Fig. S12) to simply quantify the TET efficiencies. The calculated static and TR-PL quenching efficiencies (Q_{PL} and $Q_{TR\text{-}PL}$) are summarized in Table 2. Indeed, 9-ACA quenches the PL of CdSe NCs more efficiently than 2-ACA.[8a] With increasing ZnS shell thicknesses, the quenching efficiencies of both 2-ACA and 9-ACA decrease. Notably, however, there is an interesting crossover between the relative quenching efficiencies of 2-ACA and 9-ACA. While 9-ACA still quenches the PL of CdSe@0.5ZnS NCs slightly more efficiently than 2-ACA, 2-ACA becomes a more efficient quencher for CdSe@1ZnS and CdSe@2ZnS NCs.

The crossover behavior observed for CdSe@ZnS NCs suggests that carrier probability densities on NC surfaces, or wavefunction squared ($|\Psi_S|^2$), indeed paly an essential role in the TET mechanism. For strongly-confined CdSe NCs $|\Psi_S|^2$ is large, whereas for relatively weakly-confined $CsPbBr_3$ NCs or shell-coated CdSe@ZnS NCs $|\Psi_S|^2$ is strongly reduced. Thus, an empirical rule is that a large $|\Psi_S|^2$ favors TET to 9-ACA over 2-ACA whereas a relatively small $|\Psi_S|^2$ does the opposite. Taking into consideration the different molecular geometries of 9-ACA and 2-ACA mentioned above, we propose the following explanations to this empirical rule.

When $|\Psi_S|^2$ is large, through-space electronic coupling between NCs and surface-anchored acceptors dominates (Fig. 3a). In this case, coupling with 9-ACA is more efficient than 2-ACA because the center of the anthracene moiety of 9-ACA is closer to NCs than that of 2-ACA (Fig. 3a). For weakly-confined or shell-coated NCs with small $|\Psi_S|^2$, through-space coupling is not as efficient. In this case, the chemical resonance effect (wavefunction delocalization) in 2-ACA, enabled by the co-planar configuration between the carboxylate and anthracene moieties, opens up an additional pathway for the coupling between NCs and 2-ACA (Fig. 3b). We call this a through-bond mechanism, with the bond referring the coordination bond between the carboxylate group and the surface atoms of NCs. The orthogonal geometry in 9-ACA disrupts the resonance and hence disables the through-bond mechanism. As a result, electronic coupling between NCs and 2-ACA is stronger than 9-ACA when $|\Psi_S|^2$ is small.

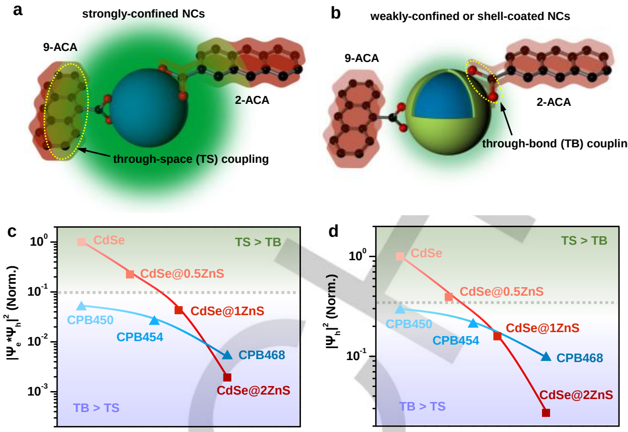

Figure 3. Through-space and through-bond TET. (a) Wavefunction leakage from strongly-confined NCs enables efficient through-space (TS) coupling with 9-ACA. (b) For weakly-confined or shell-coated NCs with weak wavefunction leakage, through-bond (TB) coupling to 2-ACA dominates over through-space coupling to 9-ACA. (c) Calculated products of electron and hole wavefunctions on NC surfaces ($|\Psi_e\Psi_h|^2$) for $CsPbBr_3$ NCs of varying sizes (blue triangles) and CdSe@ZnS NCs of varying shell thicknesses (red squares). The solid lines are guides to the eye. The green and blue shaded areas correspond to through-space and through-bond dominated regimes, respectively, separated by a gray dashed line. (d) The same plot as (c) but for calculated hole wavefunctions on NC surfaces ($|\Psi_h|^2$).

In order to verify the proposed mechanisms, we quantify the wavefunction squared on NC surfaces ($|\Psi_S|^2$) for $CsPbBr_3$ NCs of varying sizes and CdSe@ZnS NCs of varying shell thicknesses using an effective mass approximation (EMA; see SI and Table S3 for calculation details). For $CsPbBr_3$ NCs, the calculated wavefunction squared amplitudes on NC surfaces for both the electron ($|\Psi_e|^2$) and the hole ($|\Psi_h|^2$) decay with increasing NC sizes (Fig. S13). For CdSe@ZnS NCs, both $|\Psi_e|^2$ and $|\Psi_h|^2$ decay with increasing shell thicknesses, with the latter decaying more rapidly due to a larger effective mass for the hole than the electron and thus a lower hole tunneling capability (Fig. S13). In Fig. 3c, we plot the product of $|\Psi_e|^2$ and $|\Psi_h|^2$, $|\Psi_e\Psi_h|^2$, for $CsPbBr_3$ and CdSe@ZnS NCs, by scaling the value of core-only CdSe NCs to 1. From the plot, CdSe core and CdSe@0.5ZnS NCs have larger $|\Psi_e\Psi_h|^2$ than CdSe@1ZnS, CdSe@2ZnS and all the $CsPbBr_3$ NCs. This correlates well with the observations that CdSe core and CdSe@0.5ZnS NCs transfer triplet energy more efficiently to 9-ACA than to 2-ACA whereas all other NCs behave exactly oppositely. Thus, we can draw a horizontal line (gray dashed) in Fig. 3c to represent the approximate strength for the through-bond coupling pathway; above and below the line through-space and through-bond mechanisms dominate, respectively.

The use of $|\Psi_e\Psi_h|^2$ assumes a concerted mechanism for TET, *i.e.*, simultaneous transfer of the electron and the hole from NCs to ACA. However, previous studies suggest that even the one-step, direct TET process could be mediated by a virtual charge-transfer state.[9a, 22] Because of the very high reduction potential energy of ACA molecules (Fig. S8), the virtual charge-transfer state here is likely associated with hole transfer from NCs to ACA.[9a] For this reason, we present another set of analysis using $|\Psi_h|^2$ alone. As shown in Fig. 3d, in this case, $|\Psi_h|^2$ values of CdSe core and CdSe@0.5ZnS NCs still lie above those of all other NCs. Thus, regardless of the detailed TET mechanisms, we can reach the same conclusion that through-space coupling dominates in CdSe core and CdSe@0.5ZnS NCs whereas all other NCs fall in the through-bond regime.

Through-space and through-bond charge and/or energy transfer have been extensively studied in organic donor-bridge-acceptor supramolecules[23] and more recently also in inorganic/organic hybrid systems.[24] Through-bond interaction is essentially a super-exchange mechanism, which involves mixing of the donor and acceptor orbitals with the orbitals of the bridge.[23a, 25] Because both through-space and through-bond interactions should decay exponentially with the donor-acceptor distance, in many cases it is a challenge to disentangle these two mechanisms.[23a] Herein, by systematically tuning the quantum confinement strengths of inorganic NCs and by using carboxylated acceptors with or without a resonance effect, we are able to differentiate the through-space and through-bond mechanisms at the inorganic/organic interfaces.

This study provides important guidelines for the molecular design of acceptors. For strongly-confined NCs with strong wavefunction leakage onto the surfaces, the anchoring group should be functionalized at a position that allows for a maximal spatial overlap between the NC wavefunction and the molecular orbitals. In other circumstances, however, the size tuning of NCs might not be able to attain strong quantum confinement. Accordingly, anchoring groups like carboxylate should be placed at a position allowing for a co-planar molecular geometry and thus a resonance effect between the group and the molecule, in order to enable the through-bond electronic coupling mechanism.

Conclusions

In summary, we studied triplet energy transfer from $CsPbBr_3$ perovskite NCs of varying sizes and CdSe@ZnS NCs of varying shell thicknesses to surface-anchored, carboxylated anthracene isomers and the associated photon upconversion performances. We find that the NC-molecule coupling mechanisms are “through-bond” and “through-space” when the carboxyl and anthracene moieties in the molecule are co-planar or orthogonal, respectively. The relative strength of the two coupling mechanisms can be controlled by the “wavefunction-leakage” of NCs, through either NC size or shell thickness. By simultaneously engineering nanocrystal wavefunction leakage and molecular geometry, triplet energy transfer and photon upconversion efficiencies of the $CsPbBr_3$ NC/anthracene system, for example, can be improved by orders of magnitude. This study represents important progress towards a molecular-level understanding of energy migration across the inorganic/organic interface, and provides transferable guidelines for NC engineering and molecular design for efficient energy transfer useful in many applications.

Notes

The authors declare no competing financial interest.

Acknowledgments

K.W. acknowledges financial support from the National Natural Science Foundation of China (21975253, 51961165109), the Strategic Pilot Science and Technology Project of Chinese Academy of Sciences (XDA21010206), the Dalian City Foundation for Science and Technology Innovation (2018J12GX051) and Dalian Institute of Chemical Physics (DICP I201914).

Keywords: Triplet energy transfer • through-bond and through-space • perovskite nanocrystals • photon upconversion

---

[1] T. F. Schulze, T. W. Schmidt, *Energy & Environ. Sci.* **2015**, *8*, 103-125.

[2] a) T. N. Singh-Rachford, F. N. Castellano, *Coord. Chem. Rev.* **2010**, *254*, 2560-2573; b) J. Zhao, W. Wu, J. Sun, S. Guo, *Chem. Soc. Rev.* **2013**, *42*, 5323-5351.

[3] a) L. E. Brus, *J. Chem. Phys.* **1983**, *79*, 5566-5571; b) A. P. Alivisatos, *Science* **1996**, *271*, 933-937.

[4] a) M. Wu, D. N. Congreve, M. W. B. Wilson, J. Jean, N. Geva, M. Welborn, T. Van Voorhis, V. Bulović, M. G. Bawendi, M. A. Baldo, *Nat. Photon.* **2015**, *10*, 31-34; b) C. Mongin, S. Garakyaraghi, N. Razgoniaeva, M. Zamkov, F. N. Castellano, *Science* **2016**, *351*, 369-372; c) Z. Huang, M. L. Tang, *J. Am. Chem. Soc.* **2017**, *139*, 9412-9418; d) Z. Huang, X. Li, M. Mahboub, K. M. Hanson, V. M. Nichols, H. Le, M. L. Tang, C. J. Bardeen, *Nano Lett.* **2015**, *15*, 5552-5557; e) K. Okumura, K. Mase, N. Yanai, N. Kimizuka, *Chem. Eur. J.* **2016**, *22*, 7721-7726; f) N. Yanai, N. Kimizuka, *Acc. Chem. Res.* **2017**, *50*, 2487-2495; g) Z. Huang, M. L. Tang, *J. Phys. Chem. Lett.* **2018**, *9*, 6198-6206; h) L. Nienhaus, M. Wu, V. Bulović, M. A. Baldo, M. G. Bawendi, *Dalton Transactions* **2018**, *47*, 8509-8516; i) X. Luo, R. Lai, Y. Li, Y. Han, G. Liang, X. Liu, T. Ding, J. Wang, K. Wu, *J. Am. Chem. Soc.* **2019**, *141*, 4186-4190; j) S. He, X. Luo, X. Liu, Y. Li, K. Wu, *J. Phys. Chem. Lett.* **2019**, *10*, 5036-5040; k) Y. Han, S. He, X. Luo, Y. Li, Z. Chen, W. Kang, X. Wang, K. Wu, *J. Am. Chem. Soc.* **2019**, *141*, 13033-13037; l) P. Xia, E. K. Raulerson, D. Coleman, C. S. Gerke, L. Mangolini, M. L. Tang, S. T. Roberts, *Nat. Chem.* **2020**, *12*, 137-144; m) H. Lu, Z. Huang, M. S. Martinez, J. C. Johnson, J. M. Luther, M. C. Beard, *Energy & Environ. Sci.* **2020**, *13*, 1347-1376.

[5] S. Garakyaraghi, F. N. Castellano, *Inorg. Chem.* **2018**, *57*, 2351-2359.

[6] a) Z. Huang, X. Li, B. D. Yip, J. M. Rubalcava, C. J. Bardeen, M. L. Tang, *Chem. Mat.* **2015**, *27*, 7503-7507; b) M. Mahboub, H. Maghsoudiganjeh, A. M. Pham, Z. Huang, M. L. Tang, *Adv. Funct. Mater.* **2016**, *26*, 6091-6097; c) Y. Han, X. Luo, R. Lai, Y. Li, G. Liang, K. Wu, *J. Phys. Chem. Lett.* **2019**, *10*, 1457-1463.

[7] a) M. Mahboub, Z. Huang, M. L. Tang, *Nano Lett.* **2016**, *16*, 7169-7175; b) V. Gray, P. Xia, Z. Huang, E. Moses, A. Fast, D. A. Fishman, V. I. Vullev, M. Abrahamsson, K. Moth-Poulsen, M. Lee Tang, *Chem. Sci.* **2017**, *8*, 5488-5496; c) Z. Huang, Z. Xu, M. Mahboub, X. Li, J. W. Taylor, W. H. Harman, T. Lian, M. L. Tang, *Angew. Chem. Int. Ed.* **2017**, *56*, 16583-16587; d) Z. Huang, P. Xia, N. Megerdich, D. A. Fishman, V. I. Vullev, M. L. Tang, *ACS Photon.* **2018**, *5*, 3089-3096; e) M. Mahboub, P. Xia, J. Van Baren, X. Li, C. H. Lui, M. L. Tang, *ACS Energy Lett.* **2018**, 767-772.

[8] a) P. Xia, Z. Huang, X. Li, J. J. Romero, V. I. Vullev, G. S. H. Pau, M. L. Tang, *Chem. Commun.* **2017**, *53*, 1241-1244; b) J. De Roo, Z. Huang, N. J. Schuster, L. S. Hamachi, D. N. Congreve, Z. Xu, P. Xia, D. A. Fishman, T. Lian, J. S. Owen, M. L. Tang, *Chem. Mat.* **2020**, *32*, 1461-1466.

[9] a) X. Luo, Y. Han, Z. Chen, Y. Li, G. Liang, X. Liu, T. Ding, C. Nie, M. Wang, F. N. Castellano, K. Wu, *Nat. Commun.* **2020**, *11*, 28; b) X. Luo, G. Liang, Y. Han, Y. Li, T. Ding, S. He, X. Liu, K. Wu, *J. Am. Chem. Soc.* **2020**, *142*, 11270-11278.

[10] Y. Dong, T. Qiao, D. Kim, D. Parobek, D. Rossi, D. H. Son, *Nano Lett.* **2018**, *18*, 3716-3722.

[11] a) Y. Li, T. Ding, X. Luo, Z. Chen, X. Liu, X. Lu, K. Wu, *Nano Res.* **2019**, *12*, 619–623; b) Y. Li, R. Lai, X. Luo, X. Liu, T. Ding, X. Lu, K. Wu, *Chem. Sci.* **2019**, *10*, 5983-5989; c) M. C. Brennan, J. E. Herr, T. S. Nguyen-Beck, J. Zinna, S. Draguta, S. Rouvimov, J. Parkhill, M. Kuno, *J.*

Am. Chem. Soc. **2017**, *139*, 12201-12208; d) J. Maes, L. Balcaen, E. Drijvers, Q. Zhao, J. De Roo, A. Vantomme, F. Vanhaecke, P. Geiregat, Z. Hens, *J. Phys. Chem. Lett.* **2018**, *9*, 3093-3097; e) Y. Li, K. Wu, *Angew. Chem. Int. Ed.* **2020**, *10.1002/anie.202004668*.

[12] a) C. Mongin, P. Moroz, M. Zamkov, F. N. Castellano, *Nat. Chem.* **2018**, *10*, 225-230; b) H. Lu, X. Chen, J. E. Anthony, J. Johnson, M. C. Beard, *J. Am. Chem. Soc.* **2019**, *141*, 4919-4927.

[13] D. M. Kroupa, M. Vörös, N. P. Brawand, B. W. McNichols, E. M. Miller, J. Gu, A. J. Nozik, A. Sellinger, G. Galli, M. C. Beard, *Nat. Commun.* **2017**, *8*, 15257.

[14] a) W. Rodríguez-Córdoba, R. Noria-Moreno, P. Navarro, J. Peon, *J. Lumin.* **2014**, *145*, 697-707; b) T. C. Werner, T. Matthews, B. Soller, *J. Phys. Chem.* **1976**, *80*, 533-541; c) N. Ghoneim, D. Scherrer, P. Suppan, *J. Lumin.* **1993**, *55*, 271-275.

[15] X. Li, A. Fast, Z. Huang, D. A. Fishman, M. L. Tang, *Angew. Chem. Int. Ed.* **2017**, *56*, 5598-5602.

[16] M. A. Becker, R. Vaxenburg, G. Nedelcu, P. C. Sercel, A. Shabaev, M. J. Mehl, J. G. Michopoulos, S. G. Lambrakos, N. Bernstein, J. L. Lyons, T. Stöferle, R. F. Mahrt, M. V. Kovalenko, D. J. Norris, G. Rainò, A. L. Efros, *Nature* **2018**, *553*, 189-193.

[17] D. J. Norris, M. G. Bawendi, *Phys. Rev. B* **1996**, *53*, 16338-16346.

[18] L. Protesescu, S. Yakunin, M. I. Bodnarchuk, F. Krieg, R. Caputo, C. H. Hendon, R. X. Yang, A. Walsh, M. V. Kovalenko, *Nano Lett.* **2015**, *15*, 3692-3696.

[19] a) W. A. Tisdale, X.-Y. Zhu, *Proc. Natl. Acad. Sci.* **2011**, *108*, 965-970; b) H. Zhu, N. H. Song, T. Q. Lian, *J. Am. Chem. Soc.* **2010**, *132*, 15038-15045; c) H. Zhu, Y. Yang, K. Hyeon-Deuk, M. Califano, N. Song, Y. Wang, W. Zhang, O. V. Prezhdo, T. Lian, *Nano Lett.* **2014**, *14*, 1263-1269.

[20] C. Pu, J. Zhou, R. Lai, Y. Niu, W. Nan, X. Peng, *Nano Res,* **2013**, *6*, 652-670.

[21] J. De Roo, M. Ibáñez, P. Geiregat, G. Nedelcu, W. Walravens, J. Maes, J. C. Martins, I. Van Driessche, M. V. Kovalenko, Z. Hens, *ACS Nano* **2016**, *10*, 2071-2081.

[22] R. D. Harcourt, G. D. Scholes, K. P. Ghiggino, *J. Chem. Phys.* **1994**, *101*, 10521-10525.

[23] a) D. Gosztola, B. Wang, M. R. Wasielewski, *J. Photochem. Photobiol., A* **1996**, *102*, 71-80; b) M. D. Ward, *Chem. Soc. Rev.* **1997**, *26*, 365-375; c) E. A. Weiss, L. E. Sinks, A. S. Lukas, E. T. Chernick, M. A. Ratner, M. R. Wasielewski, *J. Phys. Chem. B* **2004**, *108*, 10309-10316; d) D. Bellows, T. Goudreault, S. M. Aly, D. Fortin, C. P. Gros, J.-M. Barbe, P. D. Harvey, *Organometallics* **2010**, *29*, 317-325.

[24] a) A. J. Morris-Cohen, M. D. Peterson, M. T. Frederick, J. M. Kamm, E. A. Weiss, *J. Phys. Chem. Lett.* **2012**, *3*, 2840-2844; b) X. Li, Z. Huang, R. Zavala, M. L. Tang, *J. Phys. Chem. Lett.* **2016**, *7*, 1955-1959.

[25] G. D. Scholes, K. P. Ghiggino, A. M. Oliver, M. N. Paddon-Row, *J. Am. Chem. Soc.* **1993**, *115*, 4345-4349.

10.1002/anie.202009066

Entry for the Table of Contents

Text for Table of Contents

By simultaneously engineering molecular geometry and nanocrystal wavefunction, energy transfer and photon upconversion efficiencies of a nanocrystal/molecule system can be improved by orders of magnitude.

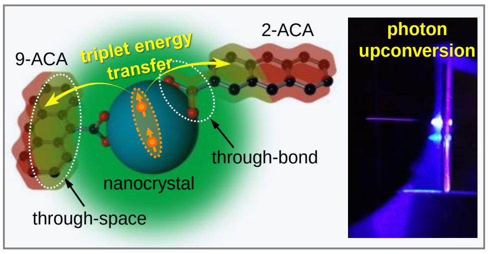

Shan He, Runchen Lai, Qike Jiang, YaoYao Han, Xiao Luo, Yuyang Tian, Xue Liu and Kaifeng Wu

Page 1-Page 6

Engineering Sensitized Photon Upconversion Efficiency via Nanocrystal Wavefunction and Molecular Geometry